High-Resolution Neutronics Model for ^{238}Pu Production in High-Flux Reactors

Qingquan PAN[1*], Qingfei ZHAO[1], Lianjie WANG[2], Bangyang XIA[2], Yun CAI[2], Jinbiao XIONG[1], Xiaojing LIU[1*]

panqingquan@sjtu.edu.cn, xiaojingliu@stu.edu.cn

1. School of Nuclear Science and Engineering
Shanghai Jiao Tong University
Shanghai, 200240, China

2. Science and Technology on Reactor System Design Technology Laboratory
Nuclear Power Institute of China
Chengdu, 610200, China

Corresponding Author: Qingquan PAN
School of Nuclear Science and Engineering
Shanghai Jiao Tong University
Shanghai, 200240, P. R. China
Email: panqingquan@sjtu.edu.cn
Tel: +0086-13751110835

Corresponding Author: Xiaojing LIU
School of Nuclear Science and Engineering
Shanghai Jiao Tong University
Shanghai, 200240, P. R. China
Email: xiaojingliu@sjtu.edu.cn
Tel: +0086-13761043485

ABSTRACT

We proposed and compared three methods (filter burnup, single-energy burnup, and burnup extremum analysis) to build a high-resolution neutronics model for ^{238}Pu production in high-flux reactors. The filter burnup and single-energy burnup methods have no theoretical approximation and can achieve a spectrum resolution of up to ~1 eV, thereby constructing the importance curve and yield curve of the full energy range. The burnup extreme analysis method combines the importance and yield curves to consider the influence of irradiation time on production efficiency, thereby constructing extreme curves. The three curves, which quantify the transmutation rate of the nuclei in each energy region, are of physical significance because they have similar distributions. A high-resolution neutronics model for ^{238}Pu production was established based on these three curves, and its universality and feasibility were proven. The neutronics model can guide the neutron spectrum optimization and improve the yield of ^{238}Pu by up to 18.81%. The neutronics model revealed the law of nuclei transmutation in all energy regions with high spectrum resolution, thus providing theoretical support for high-flux reactor design and irradiation production of ^{238}Pu.

***Keywords*:** ^{238}Pu, Neutronics model, High-flux reactor, Spectrum resolution, Spectrum optimization.

1. INTRODUCTION

Plutonium-238 (^{238}Pu) is a radioactive isotope with a half-life of 87.7 years. ^{238}Pu releases α-particles of 5.49 MeV, which are easily blocked with a range of approximately 20 μm in an aluminum plate. Meanwhile, the α-decay of ^{238}Pu produces Uranium-234 (^{234}U), which has a half-life of 2.455 × 10^5 years. Equation (1) gives the decay chain of ^{238}Pu.

$$^{238}_{94}Pu \xrightarrow{(\alpha)\quad 87.7a} {}^{234}_{92}U \xrightarrow{(\alpha)\quad 2.455\times10^5 a} {}^{230}_{90}Th \rightarrow\cdots\rightarrow {}^{206}_{82}Pb. \tag{1}$$

^{238}Pu is an ideal heat source material without the need to consider the further decay of decay daughters [1]. ^{238}Pu has a density of 19.8 g/cm^3 (25 ℃) and a heating power of 0.57 W/g, and it has been widely used in radioisotope thermoelectric generators (RTGs) [2] and radioisotope heater units, such as the general-purpose heat source radioisotope thermoelectric generator (GPHS-RTG) in Galileo spacecraft [3] and the isotopic pulse cardiac pacemakers (IPCP) [4], as shown in Figure 1.

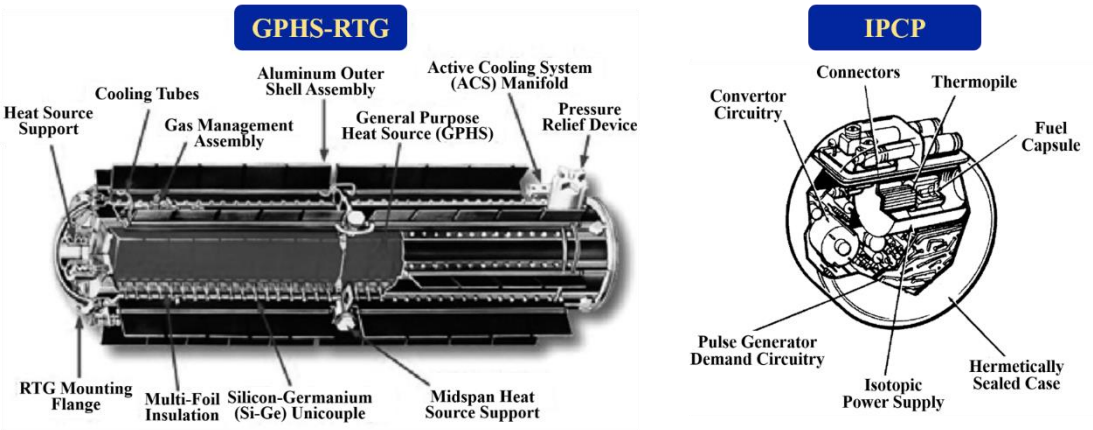

Figure 1. Structures of GPHS-RTG and IPCP

High-flux reactors [5-6] have a stable and high neutron flux, facilitating ^{238}Pu production. Two methods to produce ^{238}Pu are available: 1) in-reactor irradiation of Americium-241 (^{241}Am) [7] and 2) in-reactor irradiation of Neptunium-237 (^{237}Np) [8]. ^{238}Pu can be extracted from the decay products of Curium-242 (^{242}Cm) after the ^{241}Am target is irradiated in a reactor. Equation (2) provides the decay chain of this process.

$$^{241}_{95}Am(n,\gamma)^{242}_{95}Am \xrightarrow{\beta^-\ 16h} {}^{242}_{96}Cm \xrightarrow{\alpha\ \ 163d} {}^{238}_{94}Pu. \tag{2}$$

The purity of ^{238}Pu produced by this method is high, but this process releases strong gamma rays (59.3 eV), which deteriorate the radioactivity environment. There is almost no radioactivity problem during the production of ^{238}Pu by in-reactor irradiation of ^{237}Np. Therefore, the production of ^{238}Pu by in-reactor irradiation of ^{237}Np is a mainstream process [9]. Various nuclear reaction channels are coupled, and many new nuclides appear after the long-term irradiation of ^{237}Np targets, as shown in Figure 2. This study analyzed this production process.

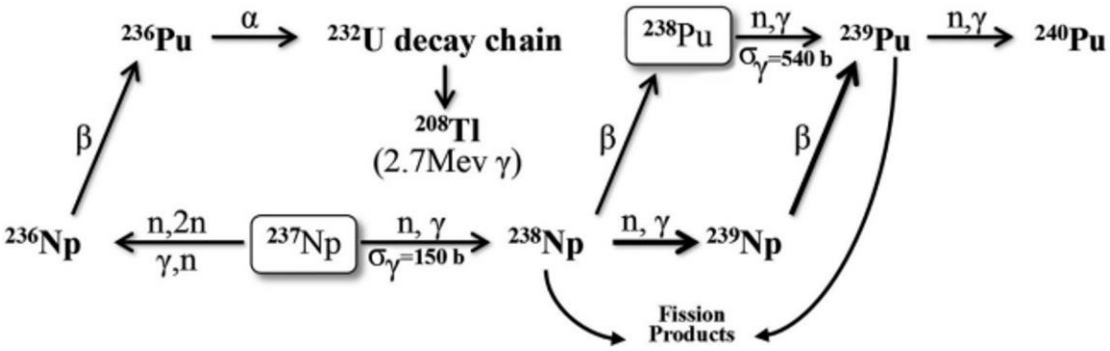

Figure 2. Nuclide transmutation path of in-reactor irradiation of ^{237}Np

The irradiation production of ^{238}Pu lacks a precise neutronics model, leading to a low transmutation rate of nuclei and high costs [10-11]. To improve production efficiency, the reactions occurring for different nuclides in the chain should be different during the irradiation period. For example, the target nuclide ^{237}Np should absorb as many neutrons as possible without any other reactions, the intermediate nuclide ^{238}Np should only undergo β-decay, and the produced ^{238}Pu should remain stable without any reaction occurring. It is difficult to regulate the nuclear reactions of the nuclide chains. The microscopic cross section of the nuclei is related to the energy spectrum [12]. Within some energy regions, the nuclide chain will have many of the required reactions, leading to a high efficiency of ^{238}Pu production, and vice versa. Therefore, neutron spectrum analysis and regulation can help increase the transmutation rates and reduce production costs. The optimization of irradiation in ^{238}Pu production can be theoretically divided into two topics: 1) determination of the optimal neutron spectrum, and 2) achievement of the optimal neutron spectrum.

Considerable research has been conducted to build neutronics models for the production of transuranic isotopes (such as ^{238}Pu and ^{252}Cf). Pan et al. [13] proposed a rapid diagnosis method for evaluating radiation schemes, which not only avoids tedious burnup calculations, but also helps provide direction for optimization. However, this method uses the initial nuclides in the target to represent all nuclides in the transmutation chain during the entire irradiation period, and only absorption and fission reactions are considered, while the other reactions (such as β-decay) cannot be considered. Pan et al. [14] defined key nuclides for neutron spectrum analysis, identified three energy regions that harm the transmutation of nuclides, and used filtering materials to reduce the neutron flux in these energy regions. However, this study did not consider the complete nuclei chain during irradiation. Hogle et al. [15-17] of the Oak Ridge National Laboratory (ORNL) presented a sensitivity curve detailing the production efficiency in each energy region. However, the analysis process was based on point-burnup calculations, resulting in a conclusion with no universality. Recently, Pan et al. [18] conducted a refined spectrum analysis of heavy nuclei synthesis in reactors, revealing the law of nuclear transmutation in all energy regions with a high spectrum resolution. However, this method has only been analyzed and verified for the synthesis of ^{252}Cf and has not been applied to other transuranic isotopes. Therefore, refined neutronics models of ^{238}Pu production are lacking.

We proposed and compared three methods for the high-resolution spectrum analysis of ^{238}Pu production in high-flux reactors. The transmutation rate of the nuclide chain in each energy region was quantified to build three relationship curves (referred to as “importance curve,” “yield curve,” and “extreme curve”) between the production efficiency and neutron spectrum. A high-resolution neutronics model for ^{238}Pu production was established. The remainder of this paper is structured as follows: Section 2 introduces the spectrum analysis, Section 3 introduces the spectrum optimization, and Section 4 concludes the paper.

2. SPECTRUM ANALYSIS

2.1 Reactor and Target

All the analyses were performed using a high-flux isotope reactor (HFIR) [19]. Rated at 100 MW and currently operating at 85 MW, the HFIR has a high steady-state neutron heat flux of 2.6×10^{15} $cm^{-2} \cdot s^{-1}$. We used a pure ^{237}Np target, a 50 cm high and 0.85 cm diameter rod placed in an irradiation channel at the neutron flux trap. The HFIR and target were modeled using the RMC code, a self-developed Monte Carlo code [20], as shown in Figure 3.

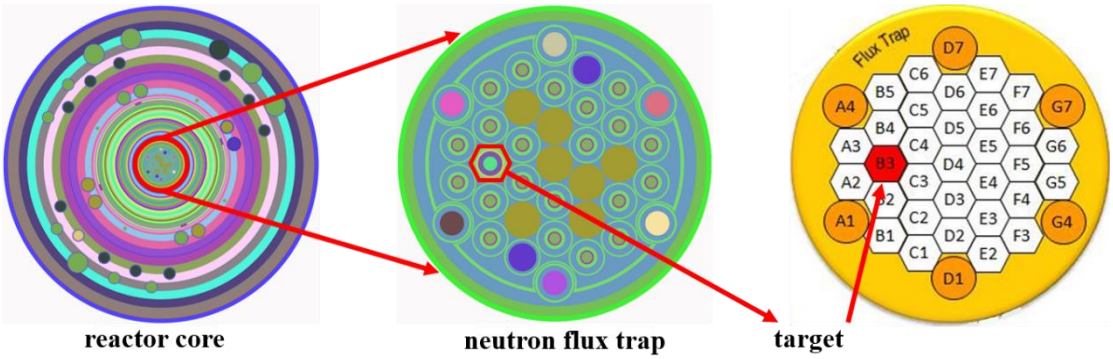

Figure 3. Modeling diagram of the high-flux isotope reactor (HFIR) and the target

2.2 Computational Method

The yield of ^{238}Pu can be obtained by performing a Monte Carlo burnup calculation, which is a coupling of the Monte Carlo criticality and point-burnup calculations. The point-burnup equation describes the transmutation of nuclides over time when a target is irradiated in a high-flux reactor. For each nuclide in the burnup chain, the time-dependent point-burnup equation can be written as

$$\frac{dn_i}{dt} = \sum_{i \neq j} b_{j,i}^{\text{eff}} \lambda_j^{\text{eff}} n_j - \lambda_i^{\text{eff}} n_i \,, \tag{1}$$

where n_i is the density of the i^{th} nuclide, λ_i^{eff} is the effective decay constant of the i^{th} nuclide, and $b_{i,j}^{\text{eff}}$ is the branching ratio for transmuting the i^{th} nuclide to the j^{th} nuclide. λ_i^{eff} and $b_{i,j}^{\text{eff}}$ can be calculated from the following formula:

$$\begin{cases} \lambda_i^{\text{eff}} = \lambda_i + \phi \sum_j \sigma_{i,j} \\ b_{i,j}^{\text{eff}} = (b_{i,j}\lambda_i + \sigma_{i,j}\phi) / \lambda_i^{\text{eff}} \end{cases}, \tag{2}$$

where λ_i is the decay constant of the i^{th} nuclide, ϕ is the neutron flux, and $\sigma_{i,j}$ is the one-group cross-sections where the i^{th} nuclide's reaction generates the j^{th} nuclide.

As shown in Equation (2), one-group cross-sections of the target are required; therefore, the Monte Carlo criticality calculation should be performed.

$$(L + C - S)\phi = \frac{1}{k\text{eff}} F\phi, \tag{3}$$

where L is the leakage operator, C is the collision operator, S is the scattering operator, F is the fission operator, and $k$eff is the effective multiplication factor. The physical parameters around the target, such as the neutron flux, fission reaction rate, and absorption reaction rate, can be obtained by solving Equation (3), which is used to determine the one-group cross-sections.

The Monte Carlo burnup calculation requires one-group cross sections integrated according to the neutron spectrum over the entire energy range rather than the cross sections in each single energy region, which can only quantify the influence of the entire neutron spectrum on the production efficiency and not a closer analysis of each single energy region. Therefore, we cannot know which energy regions are favorable and which are unfavorable for ^{238}Pu production, and thus, cannot provide a more refined theory for optimization.

We propose a filter burnup method and a single-energy burnup method for refined spectrum analysis, quantifying the transmutation rate of the nuclide chain in each energy region, and building relationship curves between the production efficiency and neutron spectrum. We also propose an extreme burnup analysis method to investigate the influence of the irradiation time on the relationship curves. Therefore, three relationship curves (importance, yield, and extreme) were obtained using the three analytical methods.

2.2.1 Filter Burnup Method

The filter burnup method seems to perform subtraction on the neutron spectrum, i.e., reducing the neutron flux in a certain energy region to investigate the relationship between the change in grouped flux and the change in yield, quantifying the importance of the flux in a certain energy region on the transmutation rate of the nuclei. Because this is a sister paper to Reference [18], the detailed theory is not repeated and only the definition of importance is provided.

$$I_i = \frac{\Delta Y_i / Y}{\Delta \phi_i} = \frac{(Y - Y_i)/Y}{\phi_i - \phi_i'} = \frac{(Y - Y_i)/Y}{M \cdot \phi_i}, \tag{4}$$

where the subscript "*i*" is the energy region index, Y and Y_i are the yields of ^{238}Pu before and after flux reduction in the *i*th energy region, respectively, ϕ and ϕ' are the grouped neutron flux before and after flux reduction, respectively, and M is the ratio of flux reduction. Previous analyses [18] have shown that the value of M (1/1, 1/2, 1/4, and 1/8) has little influence on the obtained importance curve; therefore, we take M = 1/8 directly.

The entire energy range was divided into 238 regions [21]. The energy division for the filter burnup method has no limitations, thereby achieving a high spectrum resolution. The importance of each energy region throughout the 90-day irradiation period was calculated, building up the importance curve of ^{238}Pu production, as shown in Figure 4. The ten maxima and minima in the importance curve are listed in Table 1.

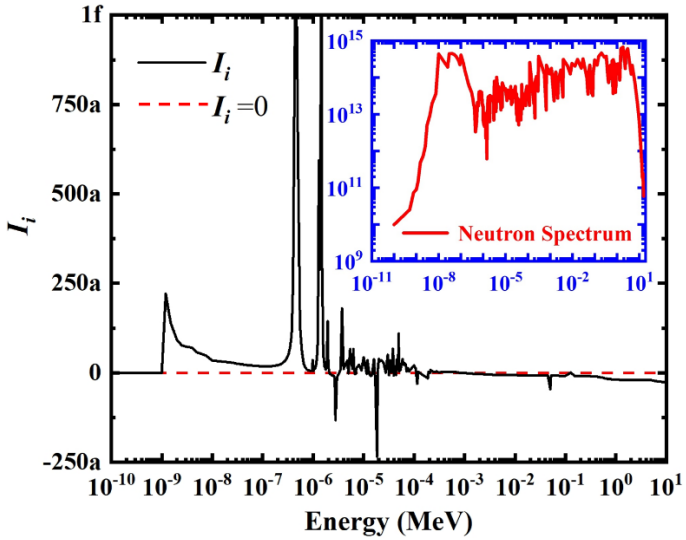

Figure 4. Importance curve of ^{238}Pu production for the filter burnup method

Table 1. Maxima and minima in the importance curve

Maximums		Minimums	
Energy Regions (MeV)	Values	Energy Regions (MeV)	Values
$[1.45\times10^{-6}, 1.50\times10^{-6}]$	1.91×10^{-15}	$[1.85\times10^{-5}, 1.90\times10^{-5}]$	-2.34×10^{-16}
$[4.50\times10^{-7}, 5.00\times10^{-7}]$	1.28×10^{-15}	$[2.77\times10^{-6}, 2.87\times10^{-6}]$	-1.33×10^{-16}
$[5.00\times10^{-7}, 5.50\times10^{-7}]$	6.18×10^{-16}	$[2.87\times10^{-6}, 2.97\times10^{-6}]$	-7.46×10^{-17}
$[1.30\times10^{-6}, 1.35\times10^{-6}]$	5.94×10^{-16}	$[5.00\times10^{-2}, 5.20\times10^{-2}]$	-4.64×10^{-17}
$[1.40\times10^{-6}, 1.45\times10^{-6}]$	5.18×10^{-16}	$[1.15\times10^{-4}, 1.19\times10^{-4}]$	-3.07×10^{-17}
$[1.50\times10^{-6}, 1.59\times10^{-6}]$	3.18×10^{-16}	$[1.00\times10^{1}, 1.28\times10^{1}]$	-2.59×10^{-17}
$[1.35\times10^{-6}, 1.40\times10^{-6}]$	2.89×10^{-16}	$[8.19\times10^{0}, 1.00\times10^{1}]$	-2.55×10^{-17}
$[4.00\times10^{-7}, 4.50\times10^{-7}]$	2.50×10^{-16}	$[6.43\times10^{0}, 8.19\times10^{0}]$	-2.38×10^{-17}
$[1.20\times10^{-9}, 1.50\times10^{-9}]$	2.21×10^{-16}	$[1.70\times10^{-5}, 1.85\times10^{-5}]$	-2.29×10^{-17}
$[1.25\times10^{-6}, 1.30\times10^{-6}]$	2.14×10^{-16}	$[1.85\times10^{0}, 2.35\times10^{0}]$	-2.10×10^{-17}

The maximum values indicate that the neutrons in these energy regions are productive, that is, increasing the neutron flux in these energy regions will increase the yield of ^{238}Pu. Meanwhile, the minima indicate that the neutrons in these energy regions are harmful, that is, increasing the neutron flux in these energy regions will decrease the yield of ^{238}Pu. Therefore, we should increase the neutron flux in the energy regions with maximum values (referred to as the "positive energy region") and reduce the neutron flux in the energy regions with minimum values (referred to as the "negative energy region") to promote the production of ^{238}Pu.

2.2.2 Single-energy Burnup Method

The single-energy burnup method does addition on the neutron spectrum, assuming that the target was irradiated with a single-energy neutron source. We simulated the ^{238}Pu production efficiency with single-energy neutron sources, that is, the total neutron flux was the same, but all neutrons were in a certain energy region. The efficiency of a certain energy region was quantified by comparing the yields of

^{238}Pu with those of single-energy neutron sources. The full energy range was divided into 238 regions, and the yields of ^{238}Pu in each energy region throughout the 90-day irradiation were calculated, thereby constructing the yield curve for the single-energy burnup method, as shown in Figure 5. The ten maximum and minimum values in the yield curve are given in Table 2.

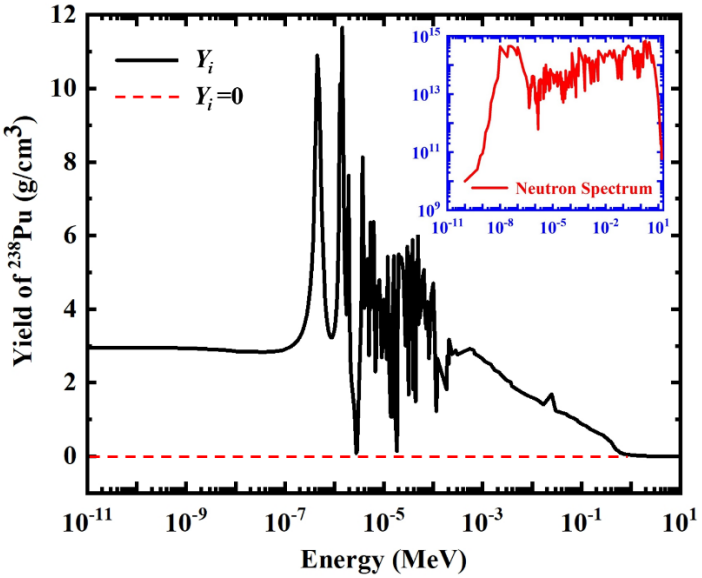

Figure 5. Yield curve of ^{238}Pu production for the single-energy burnup method

Table 2. Maxima and minima in the yield curve

Maximums		Minimums	
Energy Regions (MeV)	Values	Energy Regions (MeV)	Values
[1.45×10^{-6}, 1.50×10^{-6}]	1.17×10^{1}	[1.57×10^{1}, 1.73×10^{1}]	4.60×10^{-4}
[4.50×10^{-7}, 5.00×10^{-7}]	1.09×10^{1}	[1.73×10^{1}, 2.00×10^{1}]	4.60×10^{-4}
[1.30×10^{-6}, 1.35×10^{-6}]	1.01×10^{1}	[1.46×10^{1}, 1.57×10^{1}]	5.24×10^{-4}
[1.40×10^{-6}, 1.45×10^{-6}]	9.94×10^{0}	[1.38×10^{1}, 1.46×10^{1}]	6.04×10^{-4}
[5.00×10^{-7}, 5.50×10^{-7}]	9.84×10^{0}	[1.28×10^{1}, 1.38×10^{1}]	6.69×10^{-4}
[1.50×10^{-6}, 1.59×10^{-6}]	9.10×10^{0}	[1.00×10^{1}, 1.28×10^{1}]	8.55×10^{-4}
[1.35×10^{-6}, 1.40×10^{-6}]	8.89×10^{0}	[8.19×10^{0}, 1.00×10^{1}]	1.06×10^{-3}
[1.25×10^{-6}, 1.30×10^{-6}]	8.29×10^{0}	[6.43×10^{0}, 8.19×10^{0}]	1.51×10^{-3}
[3.73×10^{-6}, 4.00×10^{-6}]	8.14×10^{0}	[4.80×10^{0}, 6.43×10^{0}]	2.97×10^{-3}
[4.00×10^{-7}, 4.50×10^{-7}]	7.80×10^{0}	[4.30×10^{0}, 4.80×10^{0}]	3.99×10^{-3}

2.2.3 Burnup Extremum Analysis Method

The importance curve obtained using the filter burnup method and the yield curve obtained using the single-energy burnup method exhibited similar variation trends in the resonance energy range, proving the physical nature of Figures 4 and 5. However, the specific values shown in Figures 4 and 5 are inconsistent. Eight of the ten maxima in Tables 1 and 2 correspond to the same energy regions, but only three of the ten minima, which is due to the different physical assumptions of the two analysis methods. The filter burnup method perturbs a particular energy spectrum to perform a perturbation analysis that describes the importance of a particular neutron spectrum, whereas the single-energy burnup method is not limited to a particular spectrum. Taking the high-energy regions as an example, the neutrons in these regions are almost useless for ^{238}Pu production. Therefore, the yield calculated by the single-energy burnup method is zero, and the importance calculated by the filter burnup method is also zero. However, the filter burnup method can also find the energy regions that are negative for ^{238}Pu production under a particular spectral environment. Therefore, the importance can be negative numbers, which explains why only three of the ten minimum values in Tables 1 and 2 correspond to the same energy regions.

The ^{237}Np target [22] was irradiated in the neutron flux trap for 90 days using both the filter burnup and single-energy burnup methods. Significant differences in ^{238}Pu production efficiency exist among different energy regions, resulting in different irradiation times required. For some energy regions, a 90-day irradiation exceeded the time required for the yield to peak, resulting in an increase first and then a decrease in the yield during the entire irradiation period (which is referred to as “excessive irradiation”), whereas in other energy regions, a 90-day irradiation cannot lead to peak production. We used the single-energy burnup method to calculate the yields of ^{238}Pu with 5-day and 10-day irradiation to investigate the influence of the irradiation time on the yield, as shown in Figure 6.

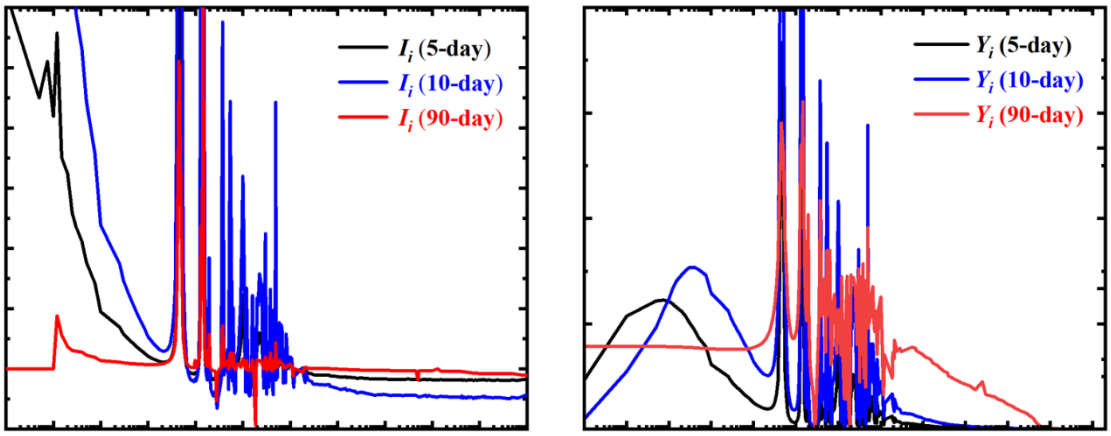

Figure 6. Comparison of curves with different irradiation times

As shown in Figure 6, different irradiation times affected the curves. We proposed a burnup extreme analysis method to eliminate the influence of irradiation time on the importance curve (Figure 4) and yield curve (Figure 5), that is, the maximum derivative between the importance (or yield) and irradiation time was calculated and used to quantify the production efficiency in the 238 energy regions, building two extreme curves, as shown in Figure 7.

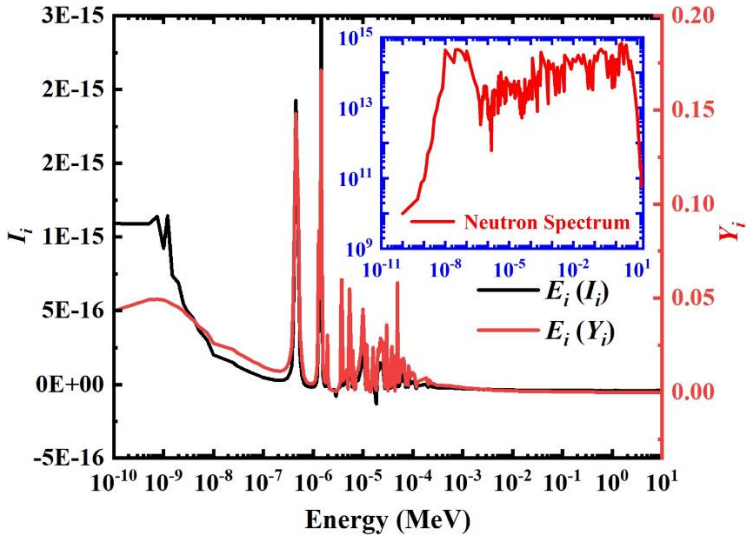

Figure 7. Two extreme curves

It can be observed that the two curves have a similar distribution trend, regardless of the analysis method. Therefore, the importance curve in Figure 4, the yield curve in Figure 5, and the extreme curves in Figure 7 have physical significance and can jointly guide the spectrum optimization for ^{238}Pu production.

2.3 Universality Testing

All curves in Section 2.2 are calculated based on the HFIR, a thermal reactor. To test the universality of these curves, we performed the same calculations in another reactor with a fast spectrum [23-32], a high-flux lead-bismuth reactor (HFLBR). Detailed parameters of this reactor can be found in a previous study [13]. As previously discussed, the filter burnup method is based on a particular neutron spectrum, whereas the single-energy burnup method is not limited to a particular neutron spectrum. Therefore, the yield curve is independent of the reactor model, whereas the importance curve is related to it. The importance curve of the HFLBR for ^{238}Pu production was calculated and compared to that of the HFIR, as shown in Figure 8. The ten maxima and minima in the importance curves are compared in Table 3.

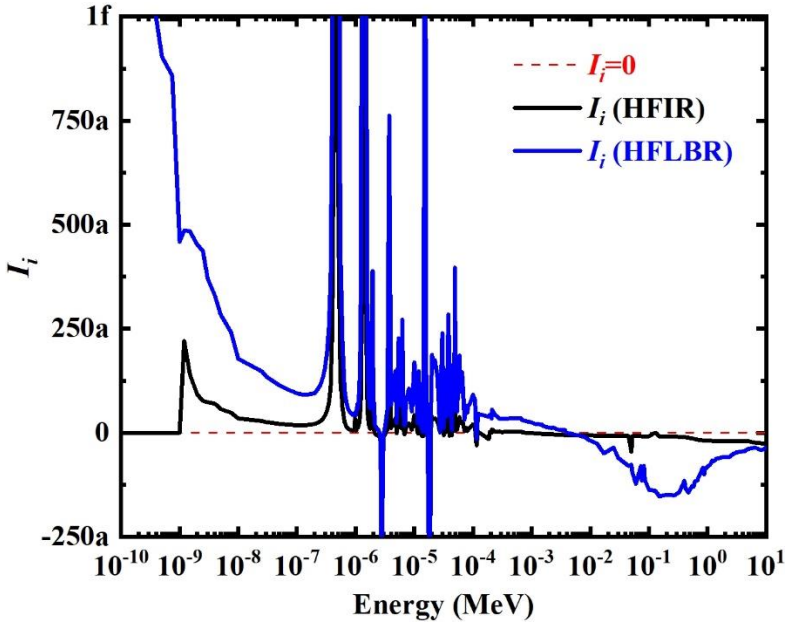

Figure 8. Importance curves of the HFLBR and HFIR

The two reactors exhibited different neutron spectra and flux levels. As shown in Figure 8, the two importance curves coincide well in the resonance-energy region and exhibit large deviations in the high- and low-energy regions, proving that the neutron spectrum influences the importance curve. However, as listed in Table 2, nine of the ten maxima and eight of the ten minima correspond to the same energy regions, proving that the importance curves are not completely dependent on the neutron spectrum and

are of physical significance, which can be used to determine the positive and negative energy regions. Therefore, the importance curve is universal and can be used for neutron spectrum optimization.

Table 3. Maxima and minima in the two importance curves

	HFIR		HFLBR	
	Energy Regions (MeV)	Values	Energy Regions (MeV)	Values
Maximum	[1.45×10^{-6}, 1.50×10^{-6}]	1.91×10^{-15}	[1.45×10^{-6}, 1.50×10^{-6}]	4.66×10^{-15}
	[4.50×10^{-7}, 5.00×10^{-7}]	1.28×10^{-15}	[4.50×10^{-7}, 5.00×10^{-7}]	3.72×10^{-15}
	[5.00×10^{-7}, 5.50×10^{-7}]	6.18×10^{-16}	[5.00×10^{-7}, 5.50×10^{-7}]	1.99×10^{-15}
	[1.30×10^{-6}, 1.35×10^{-6}]	5.94×10^{-16}	[1.40×10^{-6}, 1.45×10^{-6}]	1.97×10^{-15}
	[1.40×10^{-6}, 1.45×10^{-6}]	5.18×10^{-16}	[1.30×10^{-6}, 1.35×10^{-6}]	1.48×10^{-15}
	[1.50×10^{-6}, 1.59×10^{-6}]	3.18×10^{-16}	[1.50×10^{-6}, 1.59×10^{-6}]	1.17×10^{-15}
	[1.35×10^{-6}, 1.40×10^{-6}]	2.89×10^{-16}	[1.35×10^{-6}, 1.40×10^{-6}]	1.01×10^{-15}
	[4.00×10^{-7}, 4.50×10^{-7}]	2.50×10^{-16}	[4.00×10^{-7}, 4.50×10^{-7}]	7.45×10^{-16}
	[1.20×10^{-9}, 1.50×10^{-9}]	2.21×10^{-16}	[1.25×10^{-6}, 1.30×10^{-6}]	7.18×10^{-16}
	[1.25×10^{-6}, 1.30×10^{-6}]	2.14×10^{-16}	[3.73×10^{-6}, 4.00×10^{-6}]	7.08×10^{-16}
Minimum	[1.85×10^{-5}, 1.90×10^{-5}]	-2.34×10^{-16}	[1.85×10^{-5}, 1.90×10^{-5}]	-7.63×10^{-16}
	[2.77×10^{-6}, 2.87×10^{-6}]	-1.33×10^{-16}	[2.77×10^{-6}, 2.87×10^{-6}]	-4.20×10^{-16}
	[2.87×10^{-6}, 2.97×10^{-6}]	-7.46×10^{-17}	[2.87×10^{-6}, 2.97×10^{-6}]	-2.72×10^{-16}
	[5.00×10^{-2}, 5.20×10^{-2}]	-4.64×10^{-17}	[1.28×10^{1}, 1.38×10^{1}]	-2.34×10^{-16}
	[1.15×10^{-4}, 1.19×10^{-4}]	-3.07×10^{-17}	[1.70×10^{-5}, 1.85×10^{-5}]	-1.18×10^{-16}
	[1.00×10^{1}, 1.28×10^{1}]	-2.59×10^{-17}	[1.15×10^{-4}, 1.19×10^{-4}]	-6.58×10^{-17}
	[8.19×10^{0}, 1.00×10^{1}]	-2.55×10^{-17}	[2.67×10^{-6}, 2.77×10^{-6}]	-6.54×10^{-17}
	[6.43×10^{0}, 8.19×10^{0}]	-2.38×10^{-17}	[1.00×10^{1}, 1.28×10^{1}]	-5.02×10^{-17}
	[1.70×10^{-5}, 1.85×10^{-5}]	-2.29×10^{-17}	[8.19×10^{0}, 1.00×10^{1}]	-4.76×10^{-17}
	[1.85×10^{0}, 2.35×10^{0}]	-2.10×10^{-17}	[6.43×10^{0}, 8.19×10^{0}]	-4.47×10^{-17}

3. VERIFICATION AND APPLICATION

3.1 Neutronics Model Verification

We obtained the importance curve (Figure 4, marked as "I_i") by the filter burnup method, the yield curve (Figure 5, marked as "Y_i") by the single-energy burnup method, and the two extremes curves by the burnup extremum analysis method (Figure 7, marked as "E_i (I_i)" and "E_i (Y_i)"). These curves were used to build a high-resolution neutronics model for ^{238}Pu production in high-flux reactors, which could be used to guide neutron spectrum optimization to improve production efficiency.

To demonstrate that these curves can be used to guide the neutron spectrum optimization for ^{238}Pu production in high-flux reactors, we constructed a variety of irradiation schemes by dispersing nuclides into the target to obtain many different neutron spectra. We determined whether the yields of these irradiation schemes were positively correlated with the corresponding total spectral efficiency. The total spectrum efficiency (marked as "T") of an irradiation scheme was calculated as follows:

$$T = \sum_{i=1}^{N} \phi_i \cdot X_i , \tag{5}$$

where N is the total number of divided energy regions, ϕ_i is the neutron flux in the i^{th} energy region, X_i represents the efficiency of the i^{th} energy region, preferably I_i, Y_i, E_i (I_i), or E_i (Y_i) where T corresponds to T_1, T_2, T_3, and T_4.

The nuclides we selected included ^{107}Ag, ^{152}Eu, ^{157}Gd, ^{170}Tm, ^{161}Dy, ^{153}Eu, ^{151}Sm, ^{108}Pd, ^{140}Ba, ^{40}Ar, ^{7}Li, ^{64}Ni, ^{49}Ti, ^{151}Eu, ^{4}He, ^{138}La, ^{147}Sm, and ^{186}W. The number of nuclides added could be 10^{-2}, 10^{-3}, 10^{-4}, and 10^{-5} (in (10^{24}#/cm^3)). A total of 56 irradiation schemes were constructed. The correlation coefficients between ΔY and ΔT were calculated as follows:

$$r(\Delta Y, \Delta T_n) = \frac{Cov(\Delta Y, \Delta T_n)}{\sqrt{Var[\Delta Y] Var[\Delta T_n]}}, \qquad n = 1, 2, 3, 4 , \tag{6}$$

where ΔY is the variation of ^{238}Pu yield, ΔT is the variation of the total spectrum

efficiency, $Cov(x,y)$ is the covariance of x and y, and $Var[x]$ is the variance of x. The variation in the total spectrum efficiency T of these radiation schemes and the corresponding variation in ^{238}Pu yield are listed in Table 4.

Table 4. Variation in T and corresponding variation in ^{238}Pu yield

Nuclides	Amount	ΔY(%)	ΔT_1	ΔT_2	ΔT_3	ΔT_4
^{107}Ag	10^{-4}	0.05	8.45×10^{-3}	-3.83×10^{13}	4.78×10^{-3}	7.92×10^{9}
	10^{-5}	0.04	5.82×10^{-3}	-1.82×10^{13}	3.60×10^{-3}	3.38×10^{9}
^{152}Eu	10^{-4}	-1.50	-4.96×10^{-2}	-1.33×10^{15}	-4.24×10^{-2}	-1.95×10^{11}
	10^{-5}	0.21	1.43×10^{-3}	-2.31×10^{14}	-2.47×10^{-3}	-2.57×10^{10}
^{157}Gd	10^{-4}	-11.62	-3.31×10^{-1}	-7.70×10^{15}	-2.79×10^{-1}	-1.23×10^{12}
	10^{-5}	-2.48	-8.80×10^{-2}	-1.93×10^{15}	-7.61×10^{-2}	-3.25×10^{11}
^{170}Tm	10^{-4}	-0.20	5.40×10^{-4}	-9.66×10^{13}	1.91×10^{-4}	-6.89×10^{9}
	10^{-5}	-0.07	6.32×10^{-3}	-5.90×10^{13}	2.68×10^{-3}	7.37×10^{8}
^{161}Dy	10^{-4}	-0.11	-1.81×10^{-3}	-1.47×10^{14}	-2.23×10^{-4}	-1.20×10^{10}
	10^{-5}	-0.16	3.14×10^{-3}	-1.37×10^{14}	-5.80×10^{-4}	-1.04×10^{10}
^{153}Eu	10^{-4}	-0.07	5.08×10^{-5}	-1.14×10^{14}	2.22×10^{-3}	-2.26×10^{9}
	10^{-5}	-0.07	3.67×10^{-3}	-2.80×10^{13}	1.60×10^{-3}	2.15×10^{8}
^{151}Sm	10^{-4}	-0.22	-5.32×10^{-2}	-1.50×10^{15}	-5.04×10^{-2}	-2.29×10^{11}
	10^{-5}	-0.16	-2.14×10^{-3}	-2.46×10^{14}	-4.57×10^{-3}	-3.07×10^{10}
^{108}Pd	10^{-4}	-0.08	4.08×10^{-3}	-3.63×10^{13}	1.16×10^{-3}	-1.69×10^{9}
	10^{-5}	0.05	4.02×10^{-4}	-4.52×10^{13}	5.64×10^{-4}	-1.09×10^{9}
^{140}Ba	10^{-2}	-0.39	-4.53×10^{-2}	-1.90×10^{15}	-1.84×10^{-2}	-1.71×10^{11}
	10^{-3}	0.32	-3.05×10^{-3}	-4.52×10^{14}	4.27×10^{-4}	-3.10×10^{10}
	10^{-4}	-0.06	4.94×10^{-3}	-1.13×10^{14}	2.72×10^{-3}	-3.80×10^{9}
	10^{-5}	-0.05	1.54×10^{-3}	-4.37×10^{13}	1.57×10^{-3}	6.16×10^{8}
^{40}Ar	10^{-2}	-0.68	9.07×10^{-3}	1.12×10^{13}	4.87×10^{-3}	9.10×10^{9}
	10^{-3}	-0.11	9.96×10^{-4}	-7.68×10^{13}	1.13×10^{-3}	-1.68×10^{9}
	10^{-4}	-0.02	1.82×10^{-3}	1.30×10^{12}	2.73×10^{-3}	3.75×10^{9}
	10^{-5}	0.01	1.68×10^{-4}	-1.04×10^{14}	1.95×10^{-3}	-4.00×10^{9}
^{7}Li	10^{-2}	-0.70	9.71×10^{-4}	2.69×10^{13}	1.00×10^{-3}	8.71×10^{9}
	10^{-3}	-0.08	-4.37×10^{-3}	-1.04×10^{14}	4.62×10^{-4}	-6.63×10^{9}
	10^{-4}	-0.10	8.55×10^{-3}	-4.90×10^{13}	4.14×10^{-3}	2.04×10^{-9}
	10^{-5}	-0.11	1.51×10^{-4}	-4.18×10^{13}	-1.09×10^{-4}	-3.68×10^{9}

^{64}Ni	10^{-2}	-0.70	1.25×10^{-3}	2.92×10^{13}	3.56×10^{-3}	8.88×10^{9}
	10^{-3}	-0.14	6.81×10^{-3}	-1.08×10^{14}	1.20×10^{-4}	-1.02×10^{10}
	10^{-4}	-0.08	-2.32×10^{-4}	-2.80×10^{13}	6.53×10^{-4}	2.87×10^{9}
	10^{-5}	-0.11	4.52×10^{-4}	-1.07×10^{14}	1.81×10^{-4}	-7.04×10^{9}
^{49}Ti	10^{-2}	-0.61	3.98×10^{-3}	8.77×10^{13}	4.48×10^{-3}	1.19×10^{10}
	10^{-3}	0.01	2.94×10^{-3}	-2.84×10^{11}	3.28×10^{-3}	6.06×10^{9}
	10^{-4}	-0.06	7.71×10^{-3}	-9.80×10^{12}	8.98×10^{-4}	3.24×10^{8}
	10^{-5}	-0.05	6.60×10^{-3}	-3.74×10^{13}	1.20×10^{-3}	-1.09×10^{9}
^{151}Eu	10^{-2}	-1.34	-4.43×10^{-2}	-1.15×10^{15}	-3.48×10^{-2}	-1.62×10^{11}
	10^{-3}	-0.24	1.80×10^{-3}	-1.89×10^{14}	-7.86×10^{-4}	-1.66×10^{10}
	10^{-4}	-5.46	-1.75×10^{-1}	-4.13×10^{15}	-1.34×10^{-1}	-6.03×10^{11}
	10^{-5}	-0.69	-2.38×10^{-2}	-6.42×10^{14}	-1.55×10^{-2}	-8.29×10^{10}
^{4}He	10^{-2}	-0.66%	1.07×10^{-3}	1.59×10^{13}	1.76×10^{-3}	4.09×10^{9}
	10^{-3}	-0.06	-2.15×10^{-3}	-1.25×10^{14}	8.74×10^{-4}	-6.80×10^{9}
	10^{-4}	-0.13	-1.99×10^{-4}	-1.12×10^{14}	6.50×10^{-4}	-8.23×10^{9}
	10^{-5}	-0.18	-1.90×10^{-3}	-9.50×10^{13}	-9.98×10^{-4}	-1.12×10^{10}
^{138}La	10^{-2}	-1.33	-2.73×10^{-2}	-1.21×10^{15}	-1.80×10^{-2}	-1.34×10^{11}
	10^{-3}	-0.07	6.75×10^{-4}	-1.96×10^{14}	1.46×10^{-4}	-1.99×10^{10}
	10^{-4}	-0.02	5.25×10^{-3}	-6.28×10^{13}	2.54×10^{-3}	-2.08×10^{9}
	10^{-5}	-0.14	-2.00×10^{-5}	-5.80×10^{13}	2.16×10^{-3}	2.08×10^{9}
^{147}Sm	10^{-2}	-0.39	-4.53×10^{-2}	-1.90×10^{15}	-1.84×10^{-2}	-1.71×10^{11}
	10^{-3}	0.32	-3.05×10^{-3}	-4.52×10^{14}	4.27×10^{-4}	-3.10×10^{10}
	10^{-4}	-0.03	9.17×10^{-3}	-1.39×10^{14}	1.12×10^{-3}	-1.05×10^{10}
	10^{-5}	-0.10	3.78×10^{-4}	-5.79×10^{13}	1.74×10^{-3}	-1.98×10^{9}
^{185}W	10^{-2}	-0.88	-3.10×10^{-2}	-9.95×10^{14}	-1.54×10^{-2}	-1.10×10^{11}
	10^{-3}	0.45	1.12×10^{-2}	-1.65×10^{14}	4.10×10^{-3}	-1.02×10^{10}
	10^{-4}	-0.03	1.03×10^{-2}	-2.71×10^{13}	3.16×10^{-3}	-1.3×10^{9}
	10^{-5}	-0.08	4.75×10^{-3}	2.90×10^{13}	2.10×10^{-3}	2.67×10^{9}
correlation coefficients between ΔY and ΔT			0.949	-0.452	0.933	0.139

As can be observed from Table 4, as the filter burnup method is based on a particular neutron spectrum, ΔY is positively correlated with ΔT_1 and ΔT_3, with correlation coefficients larger than 0.9. The single burnup method is not based on a

particular neutron spectrum, and hence ΔY is not positively correlated with ΔT_2 and ΔT_4. Therefore, the importance curve based on the filter burnup method and the extreme curve based on the importance curve can be used to guide the optimization of a particular irradiation scheme, that is, to further increase the yield of ^{238}Pu of a particular irradiation scheme. The yield curve based on the single-energy burnup method and the extreme curve based on the yield curve cannot be used to guide the optimization of a particular irradiation scheme. However, the single-energy burnup method can better determine the positive- and negative-energy regions, particularly when the neutron flux in the energy region accounts for a small amount of the total neutron flux. Therefore, the single-energy burnup method can amplify the difference in importance of the filter burnup method, which is not sufficiently explicit in some energy regions. Consequently, the two methods complement each other.

3.2 Neutronics Model Application

As shown by the importance, yield, and extreme curves, neutrons in low-energy regions are conducive to the production of ^{238}Pu. Therefore, we slowed the neutrons in the target by dispersing ^{1}H in the target and constructing thermalized neutron energy spectra. The amount of hydrogen added started from 0.0 (10^{24}#/cm^3), increased by 0.2 (10^{24}#/cm^3) each time, and ended at 3.0 (10^{24}#/cm^3), resulting in a total of 16 irradiation schemes (including the original scheme). The results of ΔY(%), T_1 and T_3 are presented in Figure 9, drawn as a dot plot.

As shown in Figure 9, the yield of ^{238}Pu can be increased by regulating the neutron spectrum around the target. In the above 16 irradiation schemes, the rate of increase in the yield of ^{238}Pu was the highest when the amount of ^{1}H added was 2.6 (10^{24}#/cm^3), reaching 18.81%. Meanwhile, the rate of increase was positively correlated with the total spectrum efficiency, implying that the yield of ^{238}Pu can be further improved by a more refined neutron spectrum optimization. Therefore, a high-resolution neutronics model based on the importance curve, yield curve, and two extreme curves can guide

the neutron spectrum optimization to improve the production efficiency of ^{238}Pu.

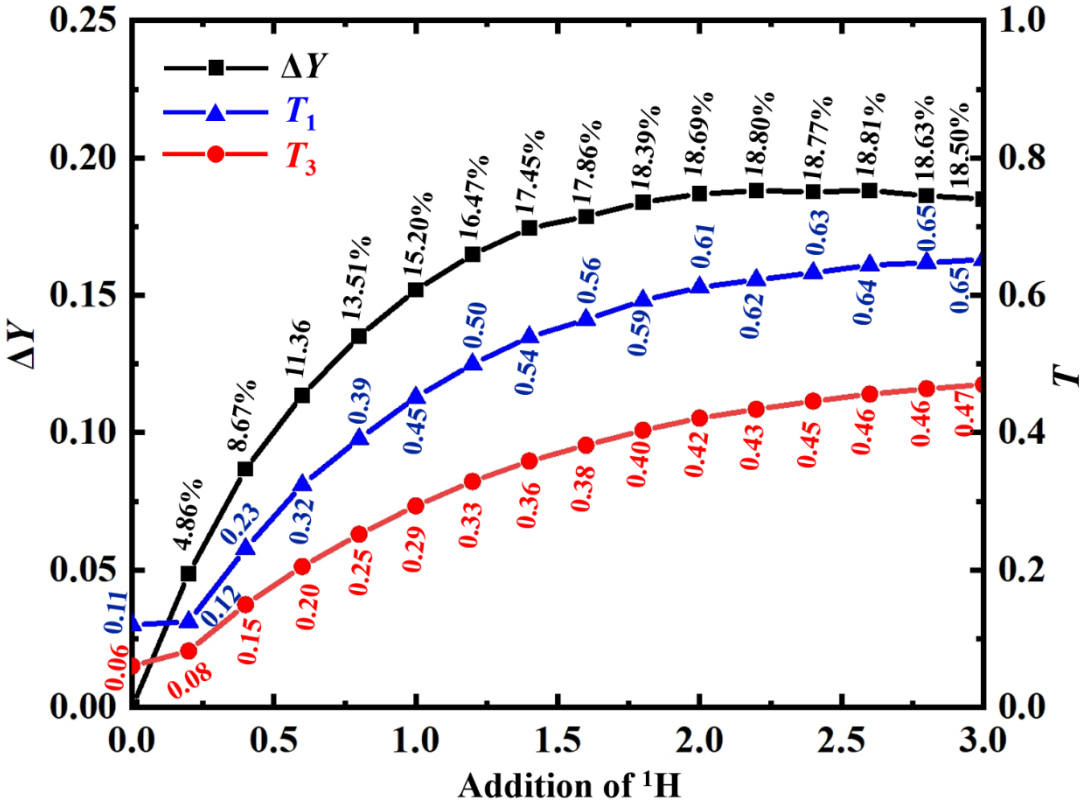

Figure 9. Results of $\Delta Y(\%)$, T_1, and T_3

4. CONCLUSION

^{238}Pu is an ideal heat source material widely used in radioisotope heater units. The production of ^{238}Pu by in-reactor irradiation of ^{237}Np is a mainstream process that involves complex nuclear transmutation. The irradiation production of ^{238}Pu lacks a precise neutronics model, which leads to a low transmutation rate of the nuclei and high costs. We proposed and compared three methods (filter burnup, single-energy burnup, and burnup extremum analysis) to build a high-resolution neutronics model for ^{238}Pu production in high-flux reactors.

The filter burnup and single-energy burnup methods have no theoretical approximation and can achieve a spectrum resolution of up to ~1 eV, thereby constructing the importance and yield curves of the full energy range. The filter burnup method is based on a particular neutron spectrum, whereas the single-energy burnup method is not limited to a particular neutron spectrum. The burnup extreme analysis method combines the importance and yield curves to consider the influence of irradiation time on production efficiency, thereby constructing extreme curves. The three curves, which quantify the transmutation rate of the nuclei in each energy region, are of physical significance because they have similar distributions. A high-resolution neutronics model for ^{238}Pu production was established based on these three curves, and its universality and feasibility were proven.

The neutronics model can guide the neutron spectrum optimization and improve the yield of ^{238}Pu by up to 18.81%. The neutronics model revealed the law of nuclei transmutation in all energy regions with high spectrum resolution, providing theoretical support for high-flux reactor design and irradiation production of ^{238}Pu. Moreover, the flowchart of the three methods for spectrum analysis is universal and can be used for the spectrum analysis of other scarce isotopes. In the future, we will conduct research on the following three aspects: (1) target design from an engineering perspective, (2) spectrum optimization based on the proposed neutronics model, and (3) irradiation channel construction for ^{238}Pu production in a high-flux reactor.

REFERENCE

[1] E.D. Collins, R.N. Morris, J.L. McDuffee et al., Plutonium-238 production program results, implications, and projections from irradiation and examination of initial NpO_2 test targets for improved production. Nucl. Technol. **208**, S18–S25 (2022). https://doi.org/10.1080/00295450.2021.2021769

[2] R.M. Ambrosi, H. Williams, E.J. Watkinson et al., European radioisotope thermoelectric generators (RTGs) and radioisotope heater units (RHUs) for space science and exploration. Space Sci. Rev. **215**, 55 (2019). https://doi.org/10.1007/s11214-019-0623-9

[3] R.C. O'Brien, R.M. Ambrosi, N.P. Bannister et al., Safe radioisotope thermoelectric generators and heat sources for space applications. J. Nucl. Mater. **377**, 506–521 (2008). https://doi.org/10.1016/j.jnucmat.2008.04.009

[4] A.A. Gage, W.M. Chardack, A.J. Federico, Clinical use of an isotopic cardiac pacemaker. Am. J. Cardiol. **33**, 138 (1974). https://doi.org/10.1016/0002-9149(74)90816-9

[5] D. Chandler, C.D. Bryan, High flux isotope reactor (HFIR). Encyclopedia of Nuclear Energy 64–73 (2021). https://doi.org/10.1016/B978-0-12-819725-7.00051-9

[6] W. Xu, J. Li, H. Xie et al., Conceptual design and safety characteristics of a new multi-mission high flux research reactor. Nucl. Sci. Tech. **34**, 34 (2023). https://doi.org/10.1007/s41365-023-01191-6

[7] A.N. Shmelev, N.I. Geraskin, G.G. Kulikov et al., The problem of large-scale production of plutonium-238 for autonomous energy sources. J. Phys.: Conf. Ser. **1689**, 012030 (2020). https://doi.org/10.1088/1742-6596/1689/1/012030

[8] C.R. Daily, J.L. McDuffee, Design studies for the optimization of ^{238}Pu production in NpO_2 targets irradiated at the high flux isotope reactor. Nucl. Technol. **206**, 1182–1194 (2020). https://doi.org/10.1080/00295450.2019.1674594

[9] H. Steven, C. Douglas, N. Jorge, et al. Economical Production of Pu-238. Idaho National Laboratory, 2013, INL/CON-11-23900. https://www.osti.gov/biblio/1082364

[10] J. Urban-Klaehn, D. Miller, B.J. Gross et al., Initial phase of Pu-238 production in Idaho National Laboratory. Appl. Radiat. Isot. **169**, 109517 (2021). https://doi.org/10.1016/j.apradiso.2020.109517

[11] G. Spencer, F. David, B. Reeder, et al. Progress on Pu-238 Production at INL From March 2021 to February 2022. Idaho National Laboratory, 2022, INL/CON-22-66710-Rev000. https://www.osti.gov/biblio/1866417

[12] M.B. Chadwick, M. Herman, P. Obložinský et al., ENDF/B-VII.1 nuclear data for science and technology: cross sections, covariances, fission product yields and decay data. Nucl. Data Sheets **112**, 2887–2996 (2011). https://doi.org/10.1016/j.nds.2011.11.002

[13] Q.Q. Pan, Q.F. Zhao, L.J. Wang et al., Rapid diagnostic method for transplutonium

isotope production in high flux reactors. Nucl. Sci. Tech. **34**, 44 (2023). https://doi.org/10.1007/s41365-023-01185-4

[14] Q.F. Zhao, Q.Q. Pan, L.J. Wang et al., Neutron spectrum optimization for Cf-252 production based on key nuclides analysis. Radiat. Phys. Chem. **214**, 111294 (2024).
https://doi.org/10.1016/j.radphyschem.2023.111294

[15] S. Hogle, C.W. Alexander, J.D. Burns et al., Sensitivity studies and experimental evaluation for optimizing transcurium isotope production. Nucl. Sci. Eng. **185**, 473–483 (2017). https://doi.org/10.1080/00295639.2016.1272973

[16] S. Hogle, G.I. Maldonado, C. Alexander, Increasing transcurium production efficiency through directed resonance shielding. Ann. Nucl. Energy **60**, 267–273 (2013).
https://doi.org/10.1016/j.anucene.2013.05.018

[17] S. Hogle. Optimization of transcurium isotope production in the High Flux Isotope Reactor. Doctoral dissertations at University of Tennessee, Knoxville, 2012.
https://trace.tennessee.edu/utk_graddiss/1529/

[18] Q. Pan, Q. Zhao, X. Liu. Spectrum Quantization Model of Heavy Nuclei Synthesis in Reactors: Taking 252Cf as an Example. Computer Physics Communications, 2024.

[19] S. Hogle, G.I. Maldonado. Modeling of the High Flux Isotope Reactor Cycle 400 with KENO-VI. Transactions of the American Nuclear Society **104**, 915 (2011). https://www.ans.org/pubs/transactions/article-12169/

[20] K. Wang, Z.G. Li, D. She et al., RMC - A Monte Carlo code for reactor core analysis. Ann. Nucl. Energy **82**, 121–129 (2015). https://doi.org/10.1016/j.anucene.2014.08.048

[21] M. Di Filippo, J. Krepel, K. Mikityuk et al., Analysis of major group structures used for nuclear reactor simulations. Proceedings of 2018 26th International Conference on Nuclear Engineering July 22–26, 2018, London, England. (2018). https://doi.org/10.1115/ICONE26-81445

[22] J. Li, J. Zhao, Z. Liu, et al. Conceptual design study on Plutonium-238 production in a multi-purpose high flux reactor. Nuclear Engineering and Technology, 2023, article in press. https://doi.org/10.1016/j.net.2023.09.019

[23] L.Y. He, S.P. Xia, X.M. Zhou et al., Th–U cycle performance analysis based on molten chloride salt and molten fluoride salt fast reactors. Nucl. Sci. Tech. **31**, 83 (2020).
https://doi.org/10.1007/s41365-020-00790-x

[24] Y. Peng, G.F. Zhu, Y. Zou et al., Neutronics physics analysis of a large fluoride-salt-cooled solid-fuel fast reactor with Th-based fuel. Nucl. Sci. Tech. **28**, 158 (2017).
https://doi.org/10.1007/s41365-017-0321-9

[25] M. Cheng, Z. Dai. Development of a three dimension multi-physics code for molten salt fast reactor. Nucl. Sci. Tech. **25**, 010601 (2014).
https://doi.org/10.13538/j.1001-8042/nst.25.010601

[26] X. Luo, C. Wang, Z.R. Zou et al., Development and application of a multi-physics and multi-scale coupling program for lead-cooled fast reactor. Nucl. Sci. Tech. **33**, 18 (2022). https://doi.org/10.1007/s41365-022-01008-y

[27] Y.N. Dai, X.T. Zheng, P.S. Ding, Review on sodium corrosion evolution of nuclear-

grade 316 stainless steel for sodium-cooled fast reactor applications. Nucl. Eng. Technol. **53**, 3474–3490 (2021). https://doi.org/10.1016/j.net.2021.05.021
[28] Z.Y. Ma, N.N. Yue, M.Y. Zheng et al., Basic verification of THACS for sodium-cooled fast reactor system analysis. Ann. Nucl. Energy **76**, 1–11 (2015). https://doi.org/10.1016/j.anucene.2014.09.025
[29] P. Song, D.L. Zhang, T.T. Feng et al., Numerical approach to study the thermal-hydraulic characteristics of Reactor Vessel Cooling system in sodium-cooled fast reactors. Prog. Nucl. Energy **110**, 213–223 (2019). https://doi.org/10.1016/j.pnucene.2018.09.021
[30] Y. Liang, D.L. Zhang, J. Zhang et al., A subchannel analysis code SACOS-Na for sodium-cooled fast reactor. Prog. Nucl. Energy **166**, 104959 (2023). https://doi.org/10.1016/j.pnucene.2023.104959
[31] P. Du, Q.W. Xiong, J.Q. Shan et al., Development and application of 3D pool-type sodium cooled fast reactor system analysis program. Prog. Nucl. Energy **144**, 104027 (2022). https://doi.org/10.1016/j.pnucene.2021.104027
[32] Y.Q. Zheng, X.N. Du, Z.T. Xu et al., SARAX: a new code for fast reactor analysis part I: Methods. Nucl. Eng. Des. **340**, 421–430 (2018). https://doi.org/10.1016/j.nucengdes.2018.10.008

Acknowledgments

Author Contributions:
All authors contributed to the study conception and design. Material preparation, data collection and analysis were performed by Qingquan PAN, Qingfei ZHAO, Lianjie WANG, Bangyang XIA, Yun CAI, Jinbiao XIONG, and Xiaojing LIU. The first draft of the manuscript was written by Qingquan PAN and all authors commented on previous versions of the manuscript. All authors read and approved the final manuscript.

Funding:
This work is sponsored by Natural Science Foundation of China [NO. 12305190], Lingchuang Research Project of China National Nuclear Corporation (CNNC), and the Science and Technology on Reactor System Design Technology Laboratory.

Conflicts of Interest:
The authors declare no conflicts of interest. We declare that we have no commercial or associative interests that represent a conflict of interest in connection with the submitted work.

Data Availability:
The data that support the findings of this study are openly available in Science Data Bank at https://cstr.cn/31253.11.sciencedb.18402
and https://doi.org/10.57760/sciencedb.18402